MP2 versus density-functional theory study of the Compton profiles of crystalline urea

Alessandro Erba,[1] Cesare Pisani,[1] Silvia Casassa,[1] Lorenzo Maschio,[1] Martin Schütz,[2] and Denis Usvyat[2]
[1]*Dipartimento di Chimica IFM and Centre of Excellence NIS (Nanostructured Interfaces and Surfaces), Università di Torino, via P. Giuria 5, I-10125 Torino, Italy*
[2]*Institute for Physical and Theoretical Chemistry, Universität Regensburg, Universitätsstrasse 31, D-93040 Regensburg, Germany*
(Received 28 December 2009; revised manuscript received 22 March 2010; published 13 April 2010)

The Compton profiles (CP) of crystalline urea are computed *ab initio* at different levels of theory and compared with accurate experimental measurements. The CRYSTAL program is used in order to collect the Hartree-Fock (HF) and density-functional theory (DFT) results, while the new CRYSCOR code is adopted for the calculation of the MP2 correction to the HF density matrix. It is demonstrated that the role of electron correlation (Fermi and Coulomb) is crucial in predicting the correct CPs; DFT is shown to provide results in partial disagreement with the experiment, at variance with the HF/MP2 treatment that correctly predicts the CP anisotropies of urea. We demonstrate that the global effect of dynamic electron correlation is the reduction of the anisotropy of the electronic momentum distribution within the crystal.

DOI: 10.1103/PhysRevB.81.165108 PACS number(s): 31.15.A−

I. INTRODUCTION

CRYSCOR is a new public code for crystalline solids, which includes Coulomb electron correlation via the wave function approach.[1] In solid-state physics applications of this kind of computational tools, special attention is obviously given to the calculated total energy, due to the importance of the related information: equilibrium geometry, relative stability of different phases, vibrational spectrum, thermodynamic properties, etc. On the other hand, energy is just a *scalar* quantity for the equilibrium configuration, the one most accessible to experimental investigations. In order to get more detailed information about the quality of the calculated ground-state solution, it may then be useful to look at observables related to the one-electron density matrix (DM), such as $\rho(\mathbf{r})$, the electron charge density (ECD), and $\pi(\mathbf{p})$, the electron momentum density (EMD), and to compare them to the experimental data. We are considering for this purpose the case of crystalline urea, for reasons explained below. The ECD, obtainable from diffraction experiments, is straightforwardly related to the topological features of the system in direct space, and thus to position of nuclei and characteristics of bonds as described, for instance, according to Bader's analysis,[2,3] and will form the object of a separate study. We are here concerned with urea's EMD, which can be obtained from directional Compton scattering experiments: as it is known, the analysis of the distribution in momentum space of the slow valence electrons can provide valuable complementary information about the chemical features of the system, in particular on hydrogen bonds and weak intermolecular interactions.

Compton scattering is in fact finding renewed interest in solid-state physics, mainly due to the progress in the experimental techniques made possible from the availability of synchrotron radiation. During the last decade, this technique has been applied to the study of many kinds of "disordered" systems like liquid water,[4–6] warm dense matter,[7] quasicrystals,[8] salt solutions,[9] etc. Yet, its main field of application still remains that of crystalline compounds, whose intrinsic anisotropy is a source of additional information: the directional Compton profiles (CP) of perovskites,[10] layered manganites,[11] NH_4F,[12] and molecular crystals like hexagonal ice,[13,14] methane hydrate,[15] urea,[16] etc. have recently been measured.

In the simulation of the CPs of crystalline materials two theoretical approaches are usually adopted, both based on an effective one-electron Hamiltonian: Kohn-Sham density-functional theory (KS-DFT) (Refs. 9, 11, 15, 17, and 18) and Hartree-Fock (HF).[12,14] DFT is by far the preferred technique in solid-state simulation studies. However, the possibility of obtaining a satisfactory description of the EMD from the KS solution is still an open question.

In fact, the occupied KS orbitals $\{\psi_j^{\mathrm{KS}}\}$ are defined so as to fulfill the condition, for closed-shell systems: $\rho(\mathbf{r}) = 2\Sigma_j |\psi_j^{\mathrm{KS}}(\mathbf{r})|^2$, where $\rho(\mathbf{r})$ is the exact ground-state ECD. In a sense, DFT is calibrated on $\rho(\mathbf{r})$, not on $\pi(\mathbf{p})$. In the KS formulation of the DFT the orbitals possess a physical meaning of *noninteracting* particles. The only link of the latter to the realistic system of *interacting* particles exists via the density in the position vector representation, which has to be the same for both systems. However, that does not hold for the density matrix and thus for the density in the momentum representation, both corresponding to the initial noninteracting particle system. Therefore, one cannot expect a good description of the momentum space density using the DFT in the KS formulation. Ragot has recently performed a detailed analysis of this topic,[19] and shown that current KS-DFT schemes lead to results worse than HF when momentum-related quantities are considered. Similar conclusions were reached by Hart and Thakkar who compared the performance of different theoretical schemes (HF, post-HF and DFT) in reproducing the EMD moments of a set of 68 closed-shell molecules:[20] generally speaking, HF performed better in this respect than DFT, and MP2 quite significantly improved the HF results.

For correcting the EMD from DFT calculations in the local density approximation (LDA), Lam and Platzman have proposed an explicit expression[21] which, however, is often overlooked; it follows that the quality of the resulting CPs is questionable.[22]

The HF method is known to correctly describe the *Fermi*

correlation among electrons exhibiting the same spin orientation and, as a consequence, to properly avoid the electronic self-interaction; furthermore, the HF EMD, at variance with DFT, is consistent with the corresponding kinetic energy. Indeed, the HF formalism provides a regular though approximate many-electron wave function, which can then be reduced to the DM either in a position or a momentum representation on the same footing. On the other hand, HF does not take into account the instantaneous *Coulomb correlation* of the electronic motions. Post-HF techniques, as available in standard codes of molecular quantum chemistry, can recover a significant portion of the Coulomb correlation: this is the case, for instance, of the Møller-Plesset perturbation theory, truncated at order n (namely, MPn), or Coupled cluster (CC) models.

The CRYSCOR code[1,23–25] implements a fully periodic MP2 method in a *local* formulation and evaluates at this level of theory the correction to both the HF energy E^{HF} and to the one-electron density matrix $\gamma^{\mathrm{HF}}(\mathbf{x};\mathbf{x}')$ of the ground state of nonconducting crystals. The HF reference solution, along with the local basis of Wannier Functions (WF) (Ref. 26–28) which span the occupied manifold, are provided by the CRYSTAL program.[29] All the quantities of interest in both programs are expressed as linear combinations of Gaussian type functions centered in the atomic nuclei: $\chi_{\mu\mathbf{g}}(\mathbf{r})$, the lattice vector $\mathbf{g}$ labeling the crystalline cell to which the atom belongs. These functions will be referred to in the following as atomic orbitals (AO).

Many applications of CRYSCOR concerning the MP2 correction to E^{HF} have been presented in the last years,[30–35] while in this work we use it for the first time for analyzing the effect of the MP2 correction to $\gamma^{\mathrm{HF}}(\mathbf{x};\mathbf{x}')$ on CPs and related quantities of a crystalline system in comparison with the experiment.

The molecular crystal of urea lends itself particularly well to this kind of analysis for various reasons:

(i) accurate directional CPs from synchrotron radiation measurements are available;[16]

(ii) urea is characterized by a variety of bonding typologies: within the molecular monomers, there are mainly covalent bonds while molecules are kept together by H bonds, electrostatic and dispersive interactions. This chemical richness provides a fine structure to the experimental CP anisotropies which is suitable for comparison with *ab initio* predictions;

(iii) currently available static structure factors experiments are not able to reveal unambiguously packing effects in the urea crystal,[36] although this should be possible with accurate experimental setups.[37] In this respect, CPs may prove to be a more sensitive probe;

(iv) in particular, intermolecular dispersive interactions could play a non-negligible role in the distribution of electron momenta. This is an important issue, in principle: as it is well known from the molecular experience and as it has recently been demonstrated also in the periodic context for many kinds of crystals,[30,33–35] the larger the importance of dispersive interactions in the system, the poorer the description provided by standard DFT while one of the strong merits of post-HF techniques is exactly that of properly taking them into account.

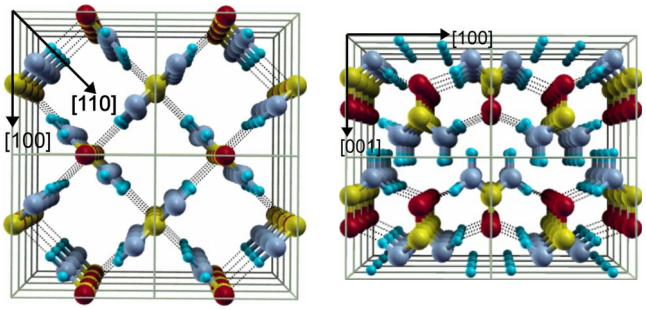

FIG. 1. (Color online) Perspective view of the structure of crystalline urea (tetragonal $P\bar{4}2_1m$ space group) through (a) the (001) family of planes and (b) the (010) family of planes. The three main crystallographic directions that will be considered in the discussion are drawn as black arrows.

Crystalline urea has been extensively studied both experimentally and theoretically: its structure is well resolved, for instance by means of neutron diffraction experiments.[38] Urea belongs to the tetragonal $P\bar{4}2_1m$ space group; the molecules are in a planar configuration (of C_{2v} point symmetry) and arrange themselves into head-to-tail planar ribbons while the planes of adjacent ribbons are orthogonal to each other and oppositely oriented (see Fig. 1).

A number of theoretical investigations were able to confirm this structure quite accurately. Reference can be made to the recent comprehensive study performed by Civalleri *et al.*,[39] which also reports about previous work on the subject. Those Authors calculated the structure and cohesive energy of crystalline urea with the CRYSTAL code at the HF level of approximation as well as using DFT with a variety of exchange-correlation potentials, either based on a local density approximation (LDA) or on a generalized gradient approximation (GGA); hybrid schemes were also tried, where a fraction of exact HF exchange is introduced.[40] The main results of that study can be summarized as follows: (i) for an unbiased evaluation of interaction energies it is essential to take the basis set superposition error into account;[41] (ii) after correction for this error, the GGA and hybrid DFT calculated geometries are in good agreement with the experimental structure, except for the a lattice vector which determines the interchain distance and is too large by about 4%; (iii) the corresponding cohesive energies underestimate the experimental value by about 30–40 kJ/mol; (iv) both the overestimation of the interchain distance and the underestimation of the cohesive energy can mainly be attributed to neglect of long-range dispersive forces;[39,42] (v) HF results are less satisfactory in all respects.

In the present work, we have tried the same one-electron Hamiltonians as in Ref. 39, plus of course HF+MP2; however, we will not present in detail the results obtained with all those DFT schemes but just the PBE (Ref. 43) and the B3LYP (Ref. 40) ones, as representatives of the GGA and of the hybrid Hamiltonians, respectively. The computational setup here adopted for the CRYSTAL calculations is also essentially the same, and corresponds to very tight tolerances. In particular, the best basis set was selected among those

tried there, with a few changes as specified in Sec. II C.

Two measurements of the directional CPs of the urea crystal have been reported so far. The first was carried out thirty years ago using a γ-ray source,[44] while the second, much more recent and accurate,[16] used synchrotron radiation. In both works, calculations were performed in order to support the interpretation of the experimental results. Reed *et al.*[44] have simulated the CPs of crystalline urea by means of molecular calculations on the isolated monomer and on the dimer in different configurations only. Shukla *et al.*[16] have performed periodic GGA-DFT calculations and subtly analyzed the effect of crystal packing with reference to the CPs of the noninteracting molecules. The results of our calculations are discussed below with reference to the data reported in those studies, especially in the more recent one. It is shown that HF provides a better description of urea's EMD than DFT, and that the MP2 correction, though small, improves the agreement with the experiment. It also confirms that CPs provide clear evidence of packing effects in the molecular crystal.

The structure of this work is as follows. Section II presents the theoretical and computational framework. After recalling the different functions which can be used for describing the EMD, their main features and the relations among them, we describe how the DM can be obtained from the present periodic calculations in the AO basis set, with particular attention to the MP2 correction. The computational setup adopted is then introduced. In Sec. III we present and discuss our results. The role of the computational parameters is first analyzed and their setup justified. In the comparison between experiment and theory, particular attention is given to the CP anisotropies which prove to be a very informative quantity. Some conclusions are drawn in Sec. IV.

II. THEORY AND COMPUTATIONAL SETUP

A. From density matrix to compton profiles

In a second-quantization formalism, the one-electron position-spin DM $\gamma(\mathbf{x};\mathbf{x}')$ associated with a normalized many-electron wave function, corresponding to the selected state $|\Psi\rangle$ can be written as follows:[45]

$$\gamma(\mathbf{x};\mathbf{x}') = \sum_{PQ} \langle\Psi|a_P^\dagger a_Q|\Psi\rangle \Phi_P^\star(\mathbf{x}')\Phi_Q(\mathbf{x}). \tag{1}$$

Here reference is made to an orthonormal set of one-electron spin-orbitals, $\Phi_Q(\mathbf{x}) \equiv \Phi_Q(\mathbf{r},\omega)$, which span the Fock space in which $|\Psi\rangle$ is defined, and $a_Q^\dagger, a_Q$ are the corresponding creation and annihilation operators. By integrating $\gamma(\mathbf{r},\omega;\mathbf{r}',\omega)$ over the spin coordinate ω, we get $R(\mathbf{r};\mathbf{r}')$, the so-called *position* DM. The *momentum* DM $P(\mathbf{p};\mathbf{p}')$ is just the six-dimensional Fourier transform of $R(\mathbf{r};\mathbf{r}')$. The ECD $\rho(\mathbf{r}) \equiv R(\mathbf{r};\mathbf{r})$ and the EMD $\pi(\mathbf{p}) \equiv P(\mathbf{p};\mathbf{p})$ are the "diagonal elements" of the position and momentum DM, respectively. By convention, the EMD $\pi(\mathbf{p})$ of a crystal is normalized to the number N_0 of electrons per cell. We note again that $\pi(\mathbf{p})$ cannot be obtained from the ECD $\rho(\mathbf{r})$, but only from the DM $R(\mathbf{r};\mathbf{r}')$. Therefore, ECD-oriented approaches, such as KS-DFT, are expected to have difficulties in correctly describing the EMD.

For the analysis and manipulation of the EMD, reference can usefully be made to the autocorrelation function (AF), $B(\mathbf{r})$, first introduced by Pattison *et al.* in 1977.[46] The AF is defined as the three-dimensional (3D) Fourier transform of the EMD or as the autocorrelation integral of the position DM,

$$B(\mathbf{r}) = \int \pi(\mathbf{p}) e^{\imath \mathbf{p}\cdot\mathbf{r}} d\mathbf{p} \equiv \frac{1}{L}\int_{\text{cyc}} R(\mathbf{r}';\mathbf{r}+\mathbf{r}')d\mathbf{r}'. \tag{2}$$

The normalization factor L is the number of cells in the cyclic crystal (cyc) determined by the Born von Kármán boundary conditions; as a consequence, the condition: $B(\mathbf{0}) = N_0$ is obeyed. It can be useful to introduce the directional AF: $B_{hkl}(r) = B(r\mathbf{e}_{hkl})$ where $\mathbf{e}_{hkl}$ is the unit vector that defines the $[hkl]$ crystallographic direction. As is shown below a lot of information can be obtained from the *AF anisotropies*, $B_{hkl}(r) - B_{h'k'l'}(r)$ or from their square modulus, which is sometimes referred to as the *power spectral density of the anisotropy*.[16]

The directional CP $J_{hkl}(p)$ can be obtained through a two-dimensional (2D) integration of $\pi(\mathbf{p})$ over a plane perpendicular to $\mathbf{e}_{hkl}$ through $p\mathbf{e}_{hkl}$, or by back-Fourier transforming the corresponding $B_{hkl}(r)$,

$$J_{hkl}(p) = \frac{1}{2\pi}\int B_{hkl}(r) e^{-\imath pr} dr. \tag{3}$$

Within the sudden-impulse approximation, this function is directly comparable to the outcome of Compton scattering experiments,[47] after correcting the latter for limited resolution and multiple scattering effects. In particular, the effect of limited resolution can be expressed as a convolution of the infinite resolution results with a normalized Gaussian function $g(p;\sigma_{cp})$ characterized by a given standard deviation σ_{cp} (or, equivalently, by the full-width-half-maximum parameter $w_{cp} = \sigma_{cp} \cdot 2\sqrt{2\log 2}$), which quantifies the experimental resolution,

$$J_{hkl}^{\sigma}(p) = \int_{-\infty}^{+\infty} J_{hkl}(p') g(p-p';\sigma_{cp}) dp'$$
$$= \int_{-\infty}^{+\infty} B_{hkl}(r) g(r,\sigma_{br}) e^{-\imath pr} dr. \tag{4}$$

In the last integrand a multiplicative Gaussian factor $g(r,\sigma_{br})$ appears, with $\sigma_{br} = 1/\sigma_{cp}$.

Although the AF and the full set of the directional CPs have the same information content, the former representation offers some distinctive advantages. First, it allows the interpretation of the EMD features in real space instead of in the less intuitive momentum space; in particular, the core electrons contribution to the AF is restricted to small $|\mathbf{r}|$'s, while at intermediate and large distances the AF is dominated by valence electrons. Furthermore, the finite resolution of the spectrometer affects the AF as a simple multiplicative factor $[B_{hkl}^{\sigma}(r) = B_{hkl}(r) g(r,\sigma_{br})]$, so its fine structure is not much affected by experimental errors. Finally, the use of Eqs. (3)

and (4) for calculating the directional CPs is computationally convenient with respect to their direct evaluation through a 2D integration of the EMD.

B. Density matrix in the AO basis set

With reference to the AO basis set $\{\chi_{\mu\mathbf{g}}(\mathbf{r})\}$ adopted in the CRYSTAL and CRYSCOR codes, the position DM can always be written as follows:

$$R(\mathbf{r};\mathbf{r}') = \sum_{\mathbf{g},\mathbf{l}} \sum_{\mu\nu} P_{\mu\nu\mathbf{g}} \chi_{\mu\mathbf{l}}(\mathbf{r}) \chi_{\nu(\mathbf{l}+\mathbf{g})}(\mathbf{r}'), \tag{5}$$

where the translational invariance of the lattice has been used.

Substitution of Eq. (5) into Eq. (2) gives

$$B(\mathbf{r}) = \sum_{\mu\nu} \sum_{\mathbf{g}} P_{\mu\nu\mathbf{g}} S_{\mu\nu\mathbf{g}}(\mathbf{r}),$$

with

$$S_{\mu\nu\mathbf{g}}(\mathbf{r}) = \int \chi_{\mu\mathbf{0}}(\mathbf{r}') \chi_{\nu\mathbf{g}}(\mathbf{r}+\mathbf{r}') d\mathbf{r}' \tag{6}$$

This computationally convenient expression for the AF is the one adopted here. From there, the infinite-resolution or the convoluted CPs are calculated using Eqs. (3) or (4), respectively.

The problem is then reduced to the estimate of $P_{\mu\nu\mathbf{g}}$. In the next two subsections we first recall how this matrix is obtained from a single-determinantal solution $|\Psi^{\mathrm{HF}}\rangle$ or $|\Psi^{\mathrm{DFT}}\rangle$, then we show how to calculate the MP2 correction to its HF estimate. The discussion is restricted to closed-shell, nonconducting crystals.

1. Density matrix from single-determinantal wave functions

The single-determinantal "X" wave function (X=HF, KS-DFT) can be expressed in two equivalent ways,

$$|\Psi^X\rangle \leftrightarrow \|\cdots \psi^X_{j,\kappa}\alpha \psi^X_{j,\kappa}\beta \cdots\| = \|\cdots w^X_{i,\mathbf{g}}\alpha w^X_{i,\mathbf{g}}\beta \cdots\|. \tag{7}$$

In the first line, the Slater determinant is constructed with the canonical doubly-occupied crystalline orbitals (CO) that satisfy the self-consistent-field equations,

$$\hat{h}^X \psi^X_{j,\kappa}(\mathbf{r}) = \varepsilon^X_{j,\kappa} \psi^X_{j,\kappa}(\mathbf{r}), \tag{8}$$

$$\psi^X_{j,\kappa}(\mathbf{r}) = \sum_{\mu} a^X_{j,\kappa;\mu} \left[\sum_{\mathbf{g}} e^{\imath\kappa\cdot\mathbf{g}} \chi_{\mu\mathbf{g}}(\mathbf{r}) \right]. \tag{9}$$

The band index j runs from 1 to $N_0/2$, while the wave vector κ is one of the L vectors in the first Brillouin zone of reciprocal space which form the Monkhorst net associated with the selected cyclic crystal. In the second line, the same determinant is expressed using the Wannier functions, labeled by $\mathbf{g}$, one of the L direct lattice vectors of the cyclic crystal, and by the in-cell index i running from 1 to $N_0/2$; the WFs are real-valued, well localized, symmetry adapted functions of $\mathbf{r}$,[27,28] which span altogether the same space as the occupied COs and are translationally equivalent and mutually orthonormal,

$$w^X_{i,\mathbf{0}}(\mathbf{r}) = w^X_{i,\mathbf{g}}(\mathbf{r}+\mathbf{g}); \tag{10}$$

$$\int w^X_{i,\mathbf{g}}(\mathbf{r}) w^X_{i',\mathbf{g}'}(\mathbf{r}) d\mathbf{r} = \delta_{ii'}\delta_{\mathbf{g}\mathbf{g}'}. \tag{11}$$

Using Eq. (1) with $|\Psi\rangle = |\Psi^X\rangle$ and making reference to the orthonormal sets $\{\Phi_Q(\mathbf{r},\omega)\}$ of the COs or of the WFs, gives us, after integration over spin,

$$R^X(\mathbf{r};\mathbf{r}') = 2\sum_{j=1}^{N_0/2} \sum_{\kappa} \psi^X_{j,\kappa}(\mathbf{r}) [\psi^X_{j,\kappa}(\mathbf{r}')]^*, \tag{12}$$

$$= 2\sum_{i=1}^{N_0/2} \sum_{\mathbf{g}} w^X_{i,\mathbf{g}}(\mathbf{r}) w^X_{i,\mathbf{g}}(\mathbf{r}'). \tag{13}$$

Substitution of Eq. (9) into Eq. (12) and comparison with Eq. (5) gives immediately,

$$P^X_{\mu\nu\mathbf{g}} = 2\sum_{j=1}^{N_0/2} \sum_{\kappa} e^{-\imath\kappa\cdot\mathbf{g}} [a^X_{j,\kappa;\mu} (a^X_{j,\kappa;\nu})^*] \tag{14}$$

We also have, by inserting Eq. (13) into Eq. (2),

$$B^X(\mathbf{r}) = 2\sum_{i=1}^{N_0/2} \int w^X_{i,\mathbf{0}}(\mathbf{r}') w^X_{i,\mathbf{0}}(\mathbf{r}+\mathbf{r}') d\mathbf{r}'$$

$$\rightarrow B^X(\mathbf{g}) = 0 \quad \forall\, \mathbf{g} \neq 0. \tag{15}$$

This important nodal property of the AF from single-determinantal wave functions of nonconducting crystals follows from the orthogonality of WFs at different lattice sites: it can be used to check the numerical accuracy of calculated AFs, and departure from it in the experimental AFs might reveal the presence of correlation effects.

2. MP2 correction to the Hartree-Fock density matrix

The MP2 level of theory provides a first-order approximation of the correlated ground-state wave function,

$$|\Psi'\rangle = \zeta(|\Psi^{\mathrm{HF}}\rangle + |\Psi^{(1)}\rangle), \tag{16}$$

where ζ is the appropriate normalization factor. This expression can be used in Eq. (1) to obtain a correlated estimate of the DM. A serious inconvenience of this approach is the lack of size consistency of the $|\Psi^{(1)}\rangle$ correction. This means that, for an "infinite" system, the DM obtained from the normalized $|\Psi'\rangle$ wave function reduces to the HF one. This deficiency has been circumvented by adopting a "local-correlation" Ansatz:[48] it consists in using a locally correlated wave function $|\Psi''\rangle$ obtained by adding to the HF solution only those biexcited configurations where at least one of the two electrons is promoted from a WF in the zero reference cell, but with excitation amplitudes obtained from the periodic MP2 calculation. The resulting DM is next periodicized. For the evaluation of the matrix elements $\langle\Psi''|a^\dagger_P a_Q|\Psi''\rangle$ reference is made to the set $\{\Phi_Q\}$ consisting of the HF WFs plus a local set of AOs orthogonalized to the occupied HF manifold and orthonormalized to each other. Reasonable results have been obtained by following this approach.[35]

A more robust technique has been implemented later in CRYSCOR by two of us,[49] and is the one adopted here. It is based on a "Lagrangian" approach,[45] according to which the DM provides the first-order response of the system energy E to an arbitrary external one-electron perturbation $\alpha\hat{X}$, with α being the strength parameter, and the one-electron operator $\hat{X}$ designated in the first quantization as $\hat{x}^c$. If $|\Psi\rangle$ were the outcome of a *variational* calculation performed for the unperturbed system, the Hellmann-Feynmann theorem,

$$\left.\frac{dE}{d\alpha}\right|_{\alpha=0} = \langle\Psi|\hat{X}|\Psi\rangle = \sum_{PQ}\langle\Psi|a_P^\dagger a_Q|\Psi\rangle\int\Phi_P^\star(\mathbf{x})\hat{x}^c\Phi_Q(\mathbf{x})d\mathbf{x} \tag{17}$$

would hold. Comparison of Eq. (17) with Eq. (1) allows us to identify here the elements R_{PQ} of the density matrix in the $\{\Phi_Q\}$ representation as the weighting factors for the matrix elements of the perturbation operator $X_{PQ}=\int\Phi_P^\star(\mathbf{x})\hat{x}^c\Phi_Q(\mathbf{x})d\mathbf{x}$ in the energy derivative expression. In a *nonvariational* treatment, as is the case for MPn or standard CC methods, the energy still can be written via a variational expression, by setting up the corresponding Lagrangian.[45] However, in this case, in addition to the excitation amplitudes which are variational parameters also in the standard variational approach, a second set of parameters is to be varied. These parameters are the Lagrange multipliers, corresponding to the MPn or CC equations used as the constraints in the Lagrangian.

In the case of MP2, the Lagrangian is nothing else than the well-known Hylleraas functional. Only the doubles amplitudes t_{ab}^{ij}, corresponding to the excitations from a pair of occupied orbitals (i,j) to a pair of virtual ones (a,b), enter the MP2 formalism. Due to the symmetric form of the Hylleraas functional, the Lagrange multipliers $\bar{t}_{ab}^{ij}$ turn out to be not independent variational parameters, but rather the contravariant amplitudes: $\bar{t}_{ab}^{ij}=2t_{ab}^{ij}-t_{ba}^{ij}$.

Next, from the resulting expression of $dE/d\alpha|_{\alpha=0}$, the weighting factors for the X_{PQ} matrix elements in analogy to Eq. (17) can be defined as the elements of the DM R_{PQ}. In case of real orthonormal orbitals $\{\phi_i(\mathbf{r})\}$, $\{\xi_a(\mathbf{r})\}$ which span the occupied and virtual HF manifold, respectively, the following expression for the MP2 correction to the HF position DM is obtained:[49]

$$R^{\mathrm{MP2}}(\mathbf{r};\mathbf{r}') = -2\sum_{kab}\bar{t}_{ab}^{jk}t_{ab}^{ik}\phi_i(\mathbf{r})\phi_j(\mathbf{r}') + 2\sum_{cij}\bar{t}_{bc}^{ij}t_{ac}^{ij}\xi_a(\mathbf{r})\xi_b(\mathbf{r}'), \tag{18}$$

This formula can be generalized to the periodic case with the occupied space spanned by Wannier functions, and the virtual space truncated according to the local approximation and represented by nonorthogonal projected atomic orbitals.[49]

An advantage of this approach is that from the size-extensive MP2 expression for the correlation energy a size-extensive correlation correction to the HF DM is obtained. Besides, its implementation turns out to be computationally more efficient than that of $\langle\Psi''|a_P^\dagger a_Q|\Psi''\rangle$. It must be pointed out that the Lagrangian DM formalism allows for a further improvement of the DM, in particular by including in the Lagrangian the constraints required for the validity of the Brillouin theorem in the presence of a perturbation, i.e., the "orbital relaxation". Presently the approach, implemented in CRYSCOR is orbital unrelaxed,[49] but the work on inclusion of the orbital relaxation effects in the DM is underway.

C. Computational setup

The present computational setup for the CRYSTAL calculations is practically the same as that adopted in Ref. 39. The only exception concerns T_1, the first of the five tolerances which control from input the truncation of the infinite lattice sums: all 1- and 2-electron integrals are neglected which involve product distributions $\Pi(\mathbf{r})=\chi_{\mu\mathbf{l}}(\mathbf{r})\chi_{\nu\mathbf{g}}(\mathbf{r})$ for which the pseudooverlap between the two AOs is less than 10^{-T_1}. It turns out that the computed AF is very sensitive to this tolerance, apparently more so for the DFT than for the HF calculations. In particular, in order to accurately satisfy the nodal property of the AF, Eq. (15), T_1 must be set to a very tight value, namely 25 instead of the default value of 6, which is adequate for most other purposes.

As concerns CRYSCOR, its input parameters serve essentially to fix three kinds of tolerances.[24] The first one determines the truncation of the support of the local functions which describe the occupied and the virtual HF manifold (WFs and projected atomic orbitals), and is here set to $t^c=0.0001$. The other parameters specify the local approximation. On the one hand, size and shape of the excitation domains must be defined for each WF; they are chosen here to extend over the whole monomer to which the WF belongs. On the other hand, two distances d_1 and d_2 are defined such that all pair interactions beyond d_2 are neglected, while d_1 controls the accuracy with which the remaining ones are treated: for WF-WF pairs with the interorbital distances d closer than d_1, the required two-electron integrals are calculated accurately by means of a periodic density fitting technique;[24,50] for the pairs with $d_1<d<d_2$, the integrals are estimated via a multipolar expansion up to hexadecapoles. In the present work the following values for these parameters have been employed: $d_1=6$ Å, $d_2=12$ Å.

Two AO basis sets are here used. The former one is of triple-ζ quality with two sets of additional polarization functions: it is obtained from the TZP set of Ref. 39 with the addition of a diffuse shell of f-type orbitals. This set indicated below as BSB, is however too demanding for the calculation of the MP2 correction to the density matrix with the present implementation of the CRYSCOR code. So, we have also used a slightly modified basis set which lacks the f polarization set, described in that same study as 6–311G(d,p), and referred to in the following as BSA. With respect to the basis sets tried in the previously cited study on the EMD moments of molecular systems (including urea),[20] BSA and BSB are essentially equivalent to "pc1" and "pc2", respectively. While the latter was shown to provide results quite close to convergence, the former is still partially inadequate. AO basis sets usually perform better with periodic than with molecular systems: in particular, the tails of the electronic distribution toward the vacuum do not there rep-

TABLE I. Position of the first minimum (r_0/Bohr) and corresponding value of the AF ($B_{hkl}(r_0)$/a.u.) for three directions and different Hamiltonians and basis sets, as indicated.

		HF		PBE		B3LYP	
		BSA	BSB	BSA	BSB	BSA	BSB
[001]	r_0	4.40	4.41	4.51	4.49	4.50	4.48
	$B(r_0)$	−0.57	−0.51	−0.62	−0.56	−0.61	−0.54
[100]	r_0	4.50	4.61	4.70	4.75	4.71	4.72
	$B(r_0)$	−0.56	−0.58	−0.48	−0.50	−0.50	−0.52
[110]	r_0	4.51	4.51	4.50	4.60	4.51	4.56
	$B(r_0)$	−0.84	−0.80	−0.88	−0.83	−0.82	−0.82

resent a principal problem. However, the basis set issue remains a critical one and will be given attention to in the following.

As already mentioned in the Introduction, we have tried many different DFT and hybrid Hamiltonians apart from HF and HF+MP2, but we will comment only on the HF, HF +MP2, PBE and B3LYP results, as representatives of the various possibilities. The experimental geometry[38] is adopted in all the present EMD calculations in order to make the comparison among the different computational results and with the experimental data easier.

III. RESULTS AND DISCUSSION

A. Autocorrelation function

Let us first analyze the directional AFs as resulting from the CRYSTAL calculations. The effect of the basis set and of the Hamiltonian on the EMD can thus be assessed; furthermore, the nodal property expressed in Eq. (15) can be verified, which is a check of the quality of the algorithms employed. The three main crystallographic directions [001], [100], and [110] are considered, the same for which the experimental CPs are available. As shown in Fig. 1, the first direction is along the ribbons and perpendicular to the other two, the second forming an angle of $\pi/4$ with the planes which contain the ribbons, the third parallel to one of the planes, and perpendicular to the other. Since in Shukla's study the AF data are provided only as anisotropies of the power spectral function and in an arbitrary scale, the comparison with the experiment is performed only at the end of this section.

For each direction, the AF starts from the value $N_0=64$ at $r=0$, reaches a deep negative minimum at a value $r_0 \approx 4.5$ Bohr, followed by a series of oscillations about zero. The position of the first minimum and the corresponding value $B_{hkl}(r_0)$ are reported in Table I for the different combinations Hamiltonian-basis set, while Fig. 2 shows the AF oscillations at longer range.

The data of Table I show that even at short range there is a considerable difference between the three directions, in particular the minimum lies deeper in the [110] direction compared to the other two. The effect of using different Hamiltonians is relevant, the PBE technique providing a much larger anisotropy than HF; the influence of the adopted basis set, though less important, is seen to be still not negligible.

The difference between the three directions becomes much more relevant at longer range, as it is evident from Fig. 2, and is qualitatively the same for the different Hamiltonians

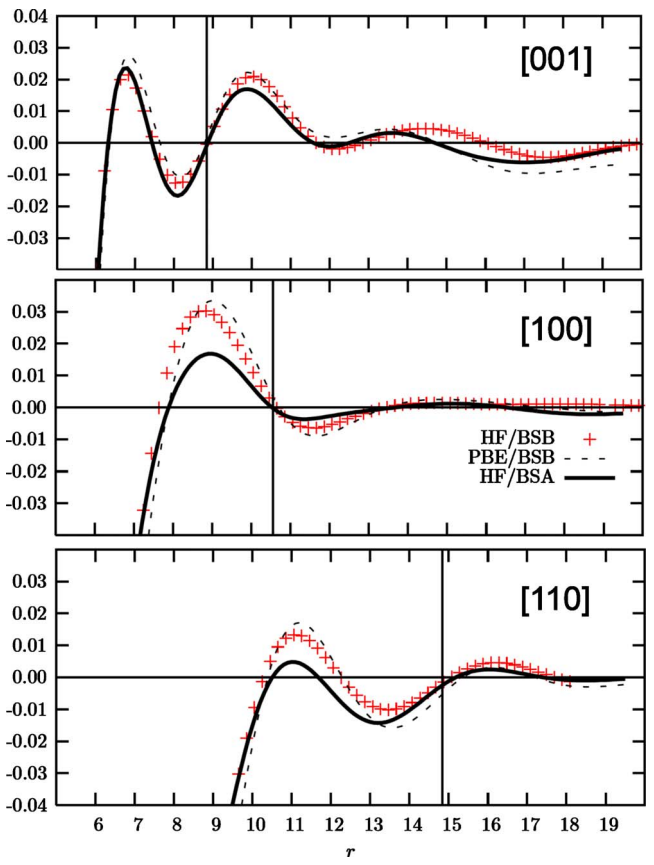

FIG. 2. (Color online) Directional AFs obtained from CRYSTAL computations using HF with basis set BSB (HF/BSB, crosses) or BSA (HF/BSA, thick continuous line), or using PBE/BSB (thin dotted line). For each considered crystallographic direction, a vertical line marks the length ℓ_{hkl} of the shortest lattice vector in that direction. Values are in atomic units.

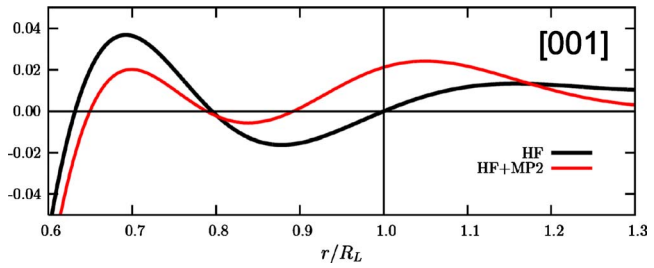

FIG. 3. (Color online) Directional AF $B_{001}(r)$ as computed at HF (black line) and HF+MP2 (red line) with the BSA basis set; the **r** coordinate has been scaled by ℓ_{001}, the length of the shortest lattice vector in that direction.

and basis sets. The region most affected is that between 7 and 15 Bohr, corresponding to the distance between opposite parts of the molecule or between the molecules. Also note that the nodal property of the AF is rather well satisfied.

It was shown in Sec. II B 1 that this property, expressed by Eq. (15), strictly depends on the single-determinantal character of the calculated wave function. The AF derived from the MP2-corrected DM, calculated following the procedure outlined in Sec. II A, no longer needs to satisfy it. The direction where this effect should be more easily observable is the [001] one, since the first lattice node occurs here at the shortest distance (ℓ_{001}) from the origin [the accuracy of the experimental $B(r)$ function is known to decrease with increasing r]. Figure 3 shows that this effect is appreciable, the zero position being displaced to a shorter distance by more than 10%. Unfortunately, a direct check of this indication against the experimental evidence is not possible, since in Ref. 16 only anisotropies are reported, not the individual directional data.

For comparison with the experiment, we provide in Fig. 4 the power spectral densities of the AF anisotropies, corresponding to those of Fig. 3 of Ref. 16: that is, after correcting the directional AFs for the limited experimental resolution, the three power density anisotropies $|B^{\sigma}_{hkl}(r)-B^{\sigma}_{h'k'l'}(r)|^2$ are reported as obtained from the use of different Hamiltonians, and using BSA for HF and HF+MP2, and BSB in the other cases (see Sec. II A for details). We first observe that the anisotropy between the [110] and the [100] directional AFs is much smaller than that between the [001] AF and either of the other two (note the different scale in the top plot). This is expected, since most of the chemical bonds are oriented along [001], and because the [100] AF corresponds in a sense to an average between that of the two orthogonal ribbon planes sampled in the [110] direction (see Fig. 1). From a comparison of the HF and HF+MP2 curve, it is seen that the overall effect of electron correlation is that of reducing the AF anisotropy.

On the whole, the data reported here look very similar to the experimental ones (see Fig. 3 of Ref. 16), which however are given in an arbitrary scale, which prevents a comparison of the absolute value of the anisotropies. A quantitative though partial comparison can be performed by considering the blow up of one of the two significant anisotropies in an intermediate region of r values (3–8 Bohr: see central panel of Fig. 4). A two-peak structure is observed in all cases, but

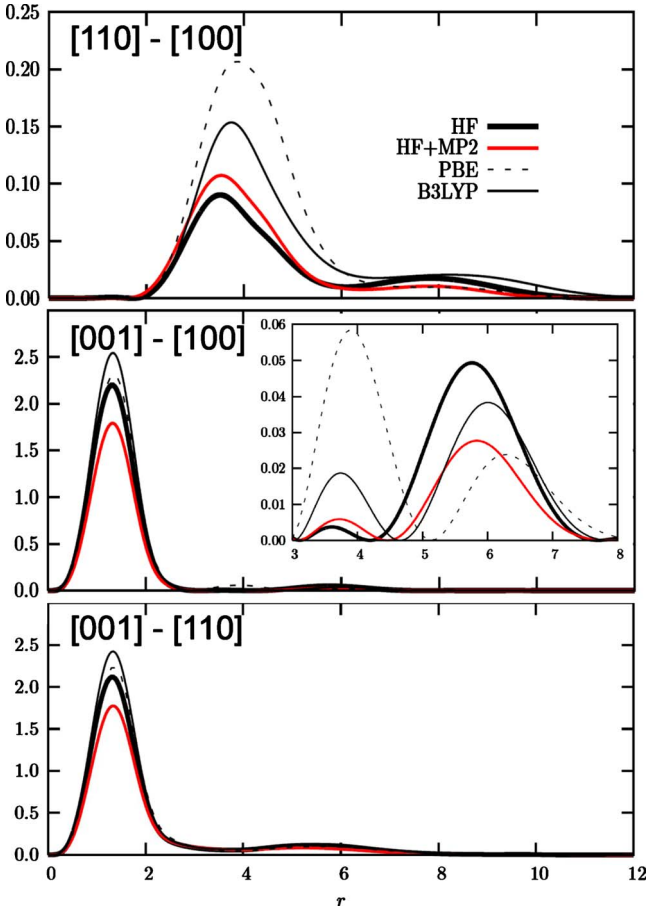

FIG. 4. (Color online) Power spectral densities of AF anisotropies. The blowup in the central panel referring to a restricted set of r values is discussed in the text. Values are in atomic units.

the relative height of the second with respect to the first peak, h_2/h_1, is very different for the various cases: 0.4, 2.0, 12.5, 4.6 for PBE, B3LYP, HF, HF+MP2, respectively. It can be noticed that the value obtained with the hybrid Hamiltonian is intermediate between the GGA-DFT and the HF values. The MP2 correction considerably reduces the h_2/h_1 ratio with respect to the HF determination, and brings it close to the experimental value, which is 4.3.

B. Compton profiles

The CPs by Shukla *et al.*[16] are characterized by a much better resolution (σ_{cp}=0.042 a.u.) than the older ones by Reed *et al.*[44] (σ_{cp}=0.193 a.u.), which is by itself indicative of their higher accuracy. Unless otherwise indicated, we shall therefore take as a reference Shukla's data, and compare them to the presently calculated ones. Since in that work only the CP anisotropies are reported, we adopt here the same representation, which not only eliminates the contribution of core electrons, but also cancels out some experimental errors such as multiple scattering effects and residual background.

Figure 5 shows the computed anisotropies corrected for limited resolution owing to the scheme outlined in Sec. II A and using σ_{cp}=0.042 a.u., so that they are directly compa-

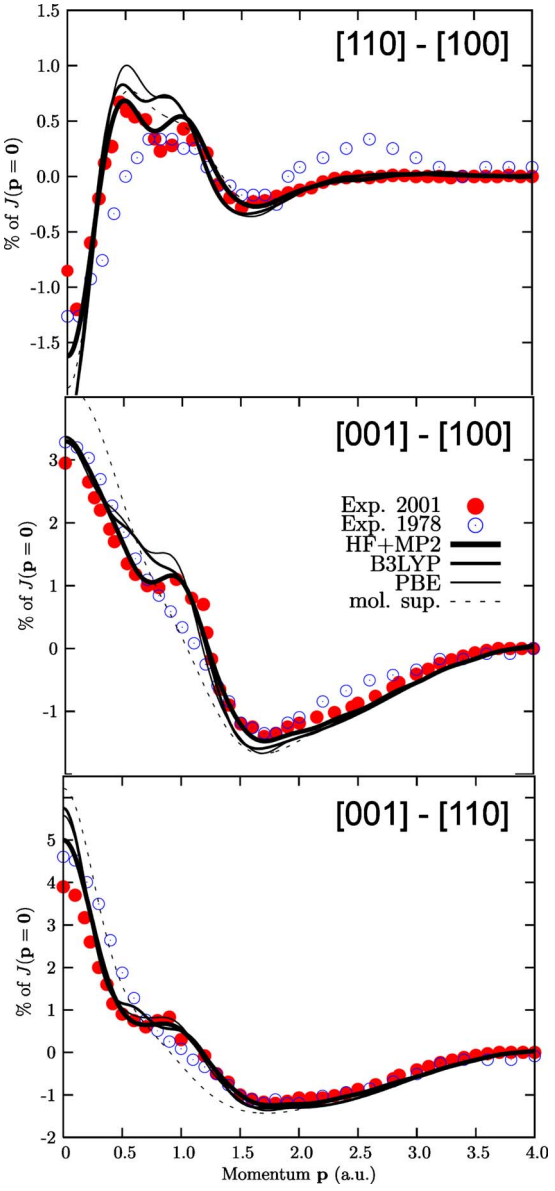

FIG. 5. (Color online) CP anisotropies as computed with several Hamiltonians using the BSB basis set (BSA for HF+MP2 calculations). Full red and empty blue circles represent experimental data by Shukla *et al.* (Ref. 16) and by Reed *et al.*, (Ref. 44), respectively; dashed lines correspond to the molecular superposition results as obtained with DFT/B3LYP (see text for more details).

rable with Shukla's data which are also given in these plots for convenience. The older data from Ref. 44 are reproduced as well, for the sake of reference; as they were obtained with a worse experimental resolution, they are not strictly comparable to the others. Finally, the CP anisotropies for the system of isolated molecules oriented as in the crystal are reported, in order to make evident the effect of intermolecular interactions. These "molecular CPs" (corrected again for limited resolution) correspond to B3LYP/BSB calculations, but the results are quite similar to those obtained with the other Hamiltonians. In Table II we provide explicitly the values of the computed CPs along the [001] direction, and the percentage anisotropies with respect to $J_{001}(0)$, again with reference to the experimental synchrotron data. The contribution of the MP2 correction to the HF CPs is displayed for the three main crystallographic directions in Fig. 6. Let us now comment on these data.

As schematically illustrated in the inset of Fig. 6, the orientation of the urea molecules within the crystal is such that all double C═O bonds and half the single N—H bonds lie almost parallel to the [001] crystallographic direction and perpendicular to the [100] and [110] directions. Since the electrons in a bond are obviously more delocalized in real space along the bond compared to the orthogonal directions, they will move more slowly in that direction: as a consequence, at low momenta, $\pi(\mathbf{p})$ will stay higher when moving along [001] than along [100] or [110]. Since a given CP is related to the EMD via a 2D integration in a plane perpendicular to the corresponding direction, in the vicinity of $p=0$, $J_{001}(p)$ is expected to be appreciably higher than either $J_{100}(p)$ or $J_{110}(p)$. This is in fact the dominating feature of the data shown in Fig. 5 and it is even more marked for the isolated molecule than for the crystal. On closer analysis, appreciable differences between the CP anisotropies of the two systems are seen to occur in a region of low momenta (0.5–1.2 a.u.) dominated by the contribution from valence electrons. In the crystalline case, they exhibit here a *fine structure* which is much more evident in Shukla's than in Reed's data, probably due to the very different resolution in the two experiments, and is also present, to a variable extent, in the theoretical results. The fact that this fine structure is absent in the "molecular" anisotropies shows how sensitive the CPs are to intermolecular interactions, as already pointed out by Shukla *et al.*[16] in the discussion of their data. The discrepancies observed in this region between the results obtained with the various Hamiltonians can then be attributed to the different description they provide of the motion of valence electrons involved in hydrogen bonds, which represent the main interaction between the urea molecules in the crystal.

From Fig. 5 it clearly comes out that the HF+MP2 method provides results in excellent agreement with the experiment, while the agreement is less satisfactory for all DFT approaches we have tried, despite the use of a better basis set. In order to explain this evidence, we could invoke the role of a correct description of the instantaneous electron correlation for a satisfactory reproduction of momentum densities. It is known that the MP2 method, taking advantage of the exact description of the electronic *Fermi correlation* (exchange) already provided by the reference HF method, can also recover a significant portion of the exact dynamic *Coulomb correlation* of the electronic motions. On the contrary, DFT describes both Fermi and Coulomb correlation as an average on the ground-state charge density and does not properly avoid electronic self-interaction; as already discussed in the Introduction, DFT is therefore not expected to perform particularly well in predicting EMDs.[19,20] Zope[51] has shown in fact that a DFT-LDA formalism corrected for self-interaction substantially improves computed CPs of atomic systems with respect to those obtained with standard GGA approaches.

The data reported in Fig. 6 allow us to better distinguish the specific role of Coulomb correlation as provided by the

TABLE II. CP of crystalline urea from (HF+MP2)/BSA, PBE/BSB, B3LYP/BSB calculations (denoted below as MP2, PBE, and hyb, respectively), and comparison with Shukla's data (Ref. 16) (exp). In the first columns the computed CPs along the [001] direction are reported (both J and p in atomic units). In the next columns the CP anisotropies are given in percentage of the value of $J_{001}(0)$: $\Delta^{\%}_{hkl-h'k'l'}(p)=[J_{hkl}(p)-J_{h'k'l'}(p)]\times 100/J_{001}(0)$. All calculated J's are convoluted for limited resolution using σ_{cp} from Ref. 16.

	J_{001}			$\Delta^{\%}_{001-100}$				$\Delta^{\%}_{001-110}$				$\Delta^{\%}_{100-110}$			
p	MP2	PBE	hyb	MP2	PBE	hyb	exp	MP2	PBE	hyb	exp	MP2	PBE	hyb	exp
0.0	24.60	24.85	24.76	3.29	3.29	3.36	2.95	4.99	5.58	5.75	3.90	−1.62	−2.16	−2.26	−0.86
0.1	24.45	24.67	24.59	3.17	3.12	3.22	2.84	4.60	5.04	5.11	3.70	−1.36	−1.81	−1.77	−1.16
0.2	24.00	24.19	24.12	2.86	2.74	2.87	2.65	3.62	3.76	3.69	2.96	−0.70	−0.94	−0.74	−0.53
0.3	23.31	23.47	23.38	2.47	2.42	2.43	2.16	2.47	2.42	2.29	1.96	0.04	0.06	0.19	0.06
0.4	22.37	22.51	22.40	2.07	2.23	2.12	1.78	1.55	1.50	1.43	1.25	0.55	0.76	0.72	0.49
0.5	21.16	21.30	21.21	1.64	2.03	1.95	1.41	0.98	1.05	1.16	0.88	0.68	1.00	0.82	0.59
0.6	19.70	19.82	19.77	1.27	1.76	1.76	1.17	0.71	0.87	1.07	0.72	0.57	0.91	0.71	0.53
0.7	18.10	18.14	18.04	1.07	1.56	1.51	0.98	0.65	0.82	0.85	0.60	0.43	0.76	0.68	0.44
0.8	16.39	16.36	16.28	1.08	1.52	1.34	0.96	0.67	0.82	0.63	0.74	0.42	0.71	0.72	0.23
0.9	14.62	14.54	14.46	1.16	1.49	1.25	1.05	0.66	0.80	0.56	0.80	0.51	0.70	0.71	0.28
1.0	12.84	12.73	12.68	1.06	1.19	1.07	0.96	0.53	0.62	0.51	0.29	0.54	0.58	0.58	0.43
1.1	11.14	10.98	10.97	0.68	0.57	0.66	0.77	0.26	0.25	0.32	0.09	0.43	0.33	0.35	0.31
1.2	9.56	9.37	9.37	0.12	−0.17	0.04	0.42	−0.09	−0.20	−0.04	−0.08	0.21	0.03	0.08	0.21
1.3	8.14	7.96	7.95	−0.44	−0.77	−0.62	−0.59	−0.44	−0.59	−0.48	−0.50	0.00	−0.19	−0.15	−0.07
1.4	6.91	6.77	6.73	−0.89	−1.16	−1.15	−0.90	−0.75	−0.88	−0.88	−0.72	−0.15	−0.30	−0.29	−0.19
1.5	5.90	5.79	5.74	−1.21	−1.43	−1.46	−1.21	−0.89	−1.11	−1.15	−1.00	−0.24	−0.35	−0.33	−0.28
1.6	5.08	4.99	4.95	−1.41	−1.61	−1.58	−1.26	−1.16	−1.28	−1.28	−1.10	−0.27	−0.36	−0.33	−0.23
1.7	4.42	4.34	4.32	−1.47	−1.67	−1.58	−1.40	−1.23	−1.36	−1.31	−1.18	−0.26	−0.33	−0.30	−0.22
1.8	3.88	3.83	3.80	−1.44	−1.59	−1.54	−1.34	−1.24	−1.35	−1.31	−1.21	−0.22	−0.26	−0.26	−0.18
1.9	3.45	3.42	3.38	−1.38	−1.48	−1.48	−1.25	−1.23	−1.32	−1.30	−1.15	−0.17	−0.19	−0.20	−0.15
2.0	3.09	3.08	3.03	−1.33	−1.41	−1.41	−1.19	−1.22	−1.31	−1.29	−1.06	−0.13	−0.14	−0.15	−0.12
2.2	2.55	2.55	2.50	−1.21	−1.29	−1.28	−1.06	−1.16	−1.26	−1.26	−1.07	−0.07	−0.05	−0.05	−0.05
2.4	2.17	2.18	2.13	−1.06	−1.10	−1.13	−0.96	−1.04	−1.13	−1.15	−0.96	−0.03	0.00	−0.01	−0.01
2.6	1.90	1.91	1.90	−0.91	−0.96	−0.95	−0.79	−0.90	−0.89	−0.99	−0.79	−0.02	0.01	0.01	−0.01
2.8	1.70	1.71	1.66	−0.71	−0.72	−0.75	−0.61	−0.73	−0.77	−0.79	−0.61	0.01	0.03	0.02	0.01
3.0	1.55	1.56	1.51	−0.54	−0.56	−0.55	−0.41	−0.57	−0.59	−0.59	−0.41	0.02	0.02	0.02	0.00
3.2	1.43	1.44	1.38	−0.36	−0.35	−0.37	−0.24	−0.40	−0.38	−0.39	−0.24	0.03	0.01	0.01	0.00
3.4	1.31	1.33	1.28	−0.22	−0.22	−0.22	−0.11	−0.24	−0.22	−0.22	−0.11	0.02	0.00	0.00	0.00
3.6	1.22	1.23	1.18	−0.10	−0.08	−0.09	−0.03	−0.11	−0.09	−0.09	−0.03	0.01	0.00	0.00	0.00
3.8	1.13	1.14	1.09	−0.01	0.01	0.00	0.00	−0.02	0.00	−0.01	0.00	0.00	0.01	0.00	0.00
4.0	1.05	1.06	1.01	0.03	0.05	0.00	0.00	0.03	0.03	0.04	0.00	0.00	0.01	0.00	0.00

MP2 correction to the description of CPs. It can first be observed that this correction is very small, since it is always within 1% of the total. Next, it is seen to be negative at low momenta and positive at high momenta for all directions. This is expected since, owing to the virial theorem, a lower total energy corresponds to a larger kinetic energy, and is a direct consequence of the fact that correlated electrons are allowed to stay closer to the nuclei and so to go faster. The third observation is that the MP2 correction to $J_{001}(p)$ is more pronounced than that to $J_{100}(p)$ and $J_{110}(p)$. This means that the electrons are more accelerated along [001] than along the orthogonal directions, due to the fact that many of the intramolecular bonds of urea are oriented parallel to the [001] direction, as schematically illustrated in the inset of Fig. 6. This suggests a global effect of electron correlation to be in the reduction in the anisotropy of the EMD of urea, as anticipated in Sec. III A. Still another kind of analysis is made possible by the local scheme implemented in CRYSCOR. Namely, we can sort out the contribution to the MP2-DM (hence to the directional CPs) associated to biexcitations of electrons in different molecules: this contribution, which is practically the same for the three directions, is represented in Fig. 6 by a thin red line. It is seen that, with respect to the HF EMD, these intermolecular terms *increase* the density of slow electrons. This may be interpreted as meaning that, contrary to what happens with electrons in ordinary chemical bonds, the Coulomb correlation slows down, on average, electrons in hydrogen bonds. Finally, the fine structure of the CP anisotropies appears to be mainly due to the HF term, with only a small contribution from the MP2 correction. This

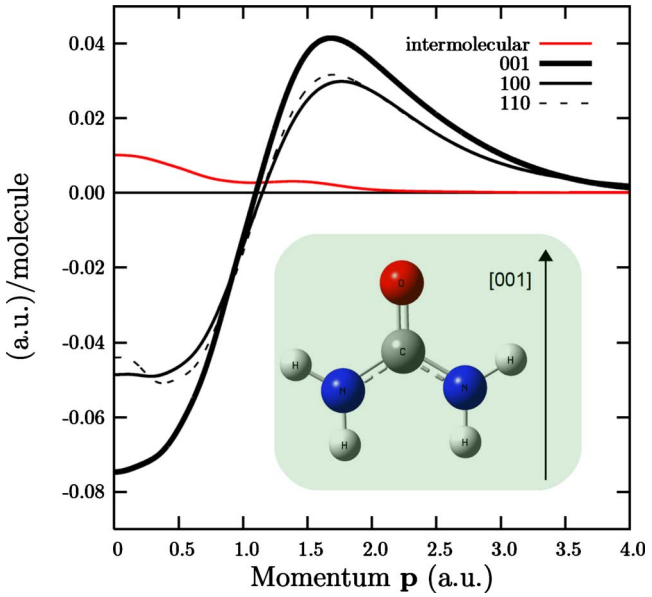

FIG. 6. (Color online) $J_{hkl}^{\mathrm{MP2}}(p)$ correction to the HF directional CPs, using the BSA basis set. The thin red curve provides the contribution to the CPs due to intermolecular interactions, and is practically the same for the three directions. The inset shows the C_{2v} planar structure of the urea molecule in the crystal and its orientation with respect to the [001] crystallographic direction.

may explain why the hybrid functional B3LYP, which contains a fraction of the HF exchange (Fermi correlation), provides an improved description of CPs with respect to pure LDA or GGA functionals.

IV. CONCLUSIONS

We have presented an *ab initio* periodic study of the Compton profiles (CP) of crystalline urea and compared our results, obtained with a variety of techniques, to recent experimental determinations. In particular, along with standard one-electron approaches (HF, DFT, and hybrid Hamiltonians) we have used here a periodic MP2 post-HF technique as implemented in the CRYSCOR code, and exploited a new feature which calculates the correlated one-electron density matrix at this level of theory.

It has been shown that CPs and their Fourier transform, the autocorrelation functions (AF), are very sensitive to intermolecular interactions, here in particular due to hydrogen bonds, and to the way these are theoretically described. This fact is particularly visible in the anisotropies of CPs and AFs between the different crystallographic directions. The DFT results, computed with different exchange-correlation functionals, are found to be generally satisfactory, but to present some definite disagreement with the experiment; this may be due to the inability of standard DFT to correctly describe the electron momentum density from which CPs are derived.[19,20] Our periodic HF+MP2 results are found to be in very good agreement with the experiment, thus demonstrating on the whole the importance of a correct description of both the Fermi and the Coulomb correlation among electrons. The main consequence of the latter is a reduction in the anisotropy of the momentum density within the crystal of urea by speeding up the valence electrons along the [001] crystallographic direction, the one which contains the majority of the intramolecular bonds. An experimentally detectable consequence of correlation effects is the shift of the AF zeros from the reticular positions, which reveals the inadequacy of a single-determinantal description for the ground state of the crystal.

Work is in progress aimed at taking into account orbital relaxation and at allowing the use of more adequate basis sets in the evaluation of the MP2 correction to the HF density matrix. We expect, however, that these technical improvements will not affect in any essential way the results here presented.

[1] C. Pisani, L. Maschio, S. Casassa, M. Halo, M. Schütz, and D. Usvyat, J. Comput. Chem. **29**, 2113 (2008); A. Erba and M. Halo, CRYSCOR09 *User's Manual*, http://www.cryscor.unito.it (2010)

[2] R. F. W. Bader, *Atoms in Molecules—A Quantum Theory* (Oxford University Press, Oxford, UK, 1990).

[3] C. Gatti, V. R. Saunders, and C. Roetti, J. Chem. Phys. **101**, 10686 (1994).

[4] M. Hakala, S. Huotari, K. Hämäläinen, S. Manninen, P. Wernet, A. Nilsson, and L. G. M. Pettersson, Phys. Rev. B **70**, 125413 (2004).

[5] M. Hakala, K. Nygård, S. Manninen, L. G. M. Pettersson, and K. Hämäläinen, Phys. Rev. B **73**, 035432 (2006).

[6] M. Hakala, K. Nygård, S. Manninen, S. Huotari, T. Buslaps, A. Nilsson, L. G. M. Pettersson, and K. Hämäläinen, J. Chem. Phys. **125**, 084504 (2006).

[7] S. Sahoo, G. F. Gribakin, G. Shabbir Naz, J. Kohanoff, and D. Riley, Phys. Rev. E **77**, 046402 (2008).

[8] J. T. Okada, Y. Watanabe, S. Nanao, R. Tamura, S. Takeuchi, Y. Yokoyama, N. Hiraoka, M. Itou, and Y. Sakurai, Phys. Rev. B **68**, 132204 (2003).

[9] K. Nygård, M. Hakala, S. Manninen, K. Hämäläinen, M. Itou, A. Andrejczuk, and Y. Sakurai, Phys. Rev. B **73**, 024208 (2006).

[10] N. Hiraoka, T. Buslaps, V. Honkimäki, H. Minami, and H. Uwe, Phys. Rev. B **71**, 205106 (2005).

[11] P. E. Mijnarends, S. Kaprzyk, B. Barbiellini, Y. Li, J. F. Mitchell, P. A. Montano, and A. Bansil, Phys. Rev. B **75**, 014428 (2007).

[12] B. Barbiellini, C. Bellin, G. Loupias, T. Buslaps, and A. Shukla, Phys. Rev. B **79**, 155115 (2009).

[13] K. Nygård, M. Hakala, S. Manninen, M. Itou, Y. Sakurai, and K. Hämäläinen, Phys. Rev. Lett. **99**, 197401 (2007).

[14] S. Ragot, J.-M. Gillet, and P. J. Becker, Phys. Rev. B **65**, 235115 (2002).

[15] C. Sternemann *et al.*, Phys. Rev. B **73**, 195104 (2006).

[16] A. Shukla, E. D. Isaacs, D. R. Hamann, and P. M. Platzman, Phys. Rev. B **64**, 052101 (2001).

[17] M. Volmer, C. Sternemann, J. S. Tse, T. Buslaps, N. Hiraoka, C. L. Bull, J. Gryko, P. F. McMillan, M. Paulus, and M. Tolan, Phys. Rev. B **76**, 233104 (2007).
[18] C. Lemell, A. Arnau, and J. Burgdörfer, Phys. Rev. B **75**, 014303 (2007).
[19] S. Ragot, J. Chem. Phys. **125**, 014106 (2006).
[20] J. R. Hart and A. J. Thakkar, Int. J. Quantum Chem. **102**, 673 (2005).
[21] L. Lam and P. M. Platzmann, Phys. Rev. B **9**, 5122 (1974).
[22] A. A. Jarzecki and E. R. Davidson, Mol. Phys. **98**, 1089 (2000).
[23] C. Pisani, M. Busso, G. Capecchi, S. Casassa, R. Dovesi, L. Maschio, C. Zicovich-Wilson, and M. Schütz, J. Chem. Phys. **122**, 094113 (2005).
[24] D. Usvyat, L. Maschio, F. R. Manby, S. Casassa, M. Schütz, and C. Pisani, Phys. Rev. B **76**, 075102 (2007).
[25] M. Schütz, D. Usvyat, M. Lorenz, C. Pisani, L. Maschio, S. Casassa, and M. Halo, in *Accurate Condensed Phase Quantum Chemistry*, edited by F. R. Manby (Taylor and Francis, New York, 2010).
[26] G. H. Wannier, Phys. Rev. **52**, 191 (1937).
[27] C. M. Zicovich-Wilson, R. Dovesi, and V. R. Saunders, J. Chem. Phys. **115**, 9708 (2001).
[28] S. Casassa, C. M. Zicovich-Wilson, and C. Pisani, Theor. Chem. Acc. **116**, 726 (2006).
[29] R. Dovesi *et al.*, CRYSTAL09 *User's Manual*, Università di Torino, Torino (2009), http://www.crystal.unito.it
[30] A. Erba, S. Casassa, L. Maschio, and C. Pisani, J. Phys. Chem. B **113**, 2347 (2009).
[31] A. Erba, S. Casassa, R. Dovesi, L. Maschio, and C. Pisani, J. Chem. Phys. **130**, 074505 (2009).
[32] C. Pisani, L. Maschio, S. Casassa, M. Halo, and A. Erba, Theor. Chem. Acc. **123**, 327 (2009).
[33] L. Maschio, D. Usvyat, M. Schütz, and B. Civalleri, J. Chem. Phys. **132**, 134706 (2010).
[34] M. Halo, S. Casassa, L. Maschio, and C. Pisani, Chem. Phys. Lett. **467**, 294 (2009).
[35] S. Casassa, M. Halo, L. Maschio, C. Roetti, and C. Pisani, Theor. Chem. Acc. **117**, 781 (2007).
[36] R. Y. de Vries, D. Feil, and V. G. Tsirelson, Acta Crystallogr., Sect. B: Struct. Sci. **56**, 118 (2000).
[37] M. A. Spackman, P. G. Byrom, M. Alfredsson, and K. Hermansson, Acta Crystallogr., Sect. A: Found. Crystallogr. **55**, 30 (1999).
[38] S. Swaminathan, B. M. Craven, M. A. Spackman, and R. F. Stewart, Acta Crystallogr., Sect. B: Struct. Sci. **40**, 398 (1984).
[39] B. Civalleri, K. Doll, and C. Zicovich-Wilson, J. Phys. Chem. B **111**, 26 (2007).
[40] A. D. Becke, J. Chem. Phys. **98**, 5648 (1993).
[41] S. Boys and F. Bernardi, Mol. Phys. **19**, 553 (1970).
[42] B. Civalleri, C. Zicovich-Wilson, L. Valenzano, and P. Ugliengo, CrystEngComm. **10**, 405 (2008).
[43] J. P. Perdew, K. Burke, and M. Ernzerhof, Phys. Rev. Lett. **77**, 3865 (1996).
[44] W. A. Reed, L. C. Snyder, H. J. Guggenheim, T. A. Weber, and Z. R. Wasserman, J. Chem. Phys. **69**, 288 (1978).
[45] T. Helgaker, P. Jørgensen, and J. Olsen, *Molecular Electronic Structure Theory* (Wiley, Chichester, UK, 2000).
[46] P. Pattison, W. Weyrich, and B. G. Williams, Solid State Commun. **21**, 967 (1977).
[47] M. Cooper, Adv. Phys. **20**, 453 (1971).
[48] C. Pisani, S. Casassa, and L. Maschio, Z. Phys. Chem. **220**, 913 (2006).
[49] D. Usvyat and M. Schütz, J. Phys.: Conf. Ser. **117**, 012027 (2008).
[50] L. Maschio and D. Usvyat, Phys. Rev. B **78**, 073102 (2008).
[51] R. R. Zope, Phys. Rev. A **62**, 064501 (2000).